Delocalized relativistic effects, from the viewpoint of halogen bonding

Serigne Sarr, Jérôme Graton, Seyfeddine Rahali, Gilles F Montavon, Nicolas Galland

Delocalized relativistic effects, from the viewpoint of halogen bonding

Serigne Sarr[a], Jérôme Graton[a], Seyfeddine Rahali[b], Gilles Montavon[c] and Nicolas Galland[a]

The ability of organic and inorganic compounds bearing both iodine and astatine atoms to form halogen-bond interactions is theoretically investigated. Upon inclusion of the relativistic spin–orbit interaction, the I-mediated halogen bonds are more affected than the At-mediated ones in many cases. This unusual outcome is disconnected from the behavior of iodine's electrons. The significant decrease of astatine electronegativity with the spin–orbit coupling triggers a redistribution of the electron density, which propagates relativistic effects toward the distant iodine atom. This mechanism can be controlled by introducing suitable substituents and, in particular, strengthened by taking advantage of electron-withdrawing inductive and mesomeric effects. Noticeable relativistic effects can actually be transferred to light atoms properties, *e.g.*, the halogen-bond basicity of bridgehead carbon atoms doubled in propellane derivatives.

1. Introduction

For more than a century, chemists have been drawing formulas where atoms are bonded by electron pairs.[1] This concept of chemical bond is incredibly simple but fruitful for the molecular structure understanding. However, the bonding in many compounds containing heavy or super-heavy atoms is still unclear to chemists. Contrary to Dirac's belief (''relativity ideas [...] are therefore of no importance in the consideration of atomic and molecular structure''),[2] it turned out that in many cases relativistic effects actually play a significant role in chemical bonding.[3] Relativistic effects are defined as the differences between properties calculated by models that consider and that do not consider relativity. They arise from electrons that experience a high nuclear charge in the core region of atoms. These electrons are then subject to special relativity, which generates spin-independent (scalar) effects and spin-dependent effects. The scalar-relativistic effects are essentially associated with the relativistic mass increase of the electrons, resulting from their high speed near the nucleus. The main spin-dependent effect is the spin–orbit coupling (SOC), *i.e.* the interaction of the electron spin with magnetic fields generated by other charged particles in relative motion, leading to the coupling between electron spin and orbital momentum.

The ability of heavy and super-heavy elements to form chemical bonds is affected by their own relativistic effects. The spatial dimension of relativistic effects at the atomic level has been investigated for a long time.[4–6] The direct effect, *i.e.* the dynamics dominated by the innermost electrons, is generally identified with the radial contraction and energetic stabilization of notably s and most p shells in atoms. In heavy and super-heavy elements, the large scalar-relativistic stabilization of the valence s orbital can lead to form an ''inert pair''. The electron-pair withdraws from the valence space, which obviously modulates the bonding properties.[7] The indirect relativistic effect is sometimes summarized to an energetic destabilization, due to the more efficient screening provided by the relativistically contracted inner core shells, and the radial expansion of the outer d and f shells. But filled relativistically expanded d and f orbitals that have tails into the core region cause also an indirect stabilization, which can compensate for valence s and p shells the above-mentioned indirect destabilization.[5] We can also report significant effects of SOC on orbitals of angular-momentum quantum numbers $l > 0$. For instance, the valence $p_{3/2}$ subshell is destabilized and expanded in contrast to the $p_{1/2}$ subshell, which is relativistically stabilized and contracted. However, the investigations of spin-dependent relativistic effects on chemical bonds are actually rather limited with respect to those studying the scalar-relativistic effects.[7,8]

This work is concerned not only by studying the SOC effects on bonding, but also by understanding effects that play far beyond the atomic horizon. While focused on astatinated compounds, we have recently uncovered some astonishing behaviors. For example, the hypoastatous acid (AtOH) can either interact with Lewis bases, through hydrogen bonds (HBs) *via* its hydrogen atom, or through halogen bonds (XBs) *via* the astatine atom. Its ability to form XBs is weakened by ~14% upon inclusion of SOC while the ability to

[a] *Université de Nantes, CNRS, CEISAM UMR 6230, 44000 Nantes, France. E-mail: nicolas.galland@univ-nantes.fr*
[b] *Department of Chemistry, College of Science and Arts, Qassim University, 51921 Ar Rass, Saudi Arabia*
[c] *IMT Atlantique, CNRS, SUBATECH UMR 6457, 44307 Nantes, France*

form HBs is weakened by ~17%.[9] Hence, the chemical properties of hydrogen, the lightest atom, appear more affected by relativistic effects than those of the much heavier astatine atom (Z = 85). In addition, it is worth noting that H and At atoms are not directly bonded in the AtOH species. The relativistic SOC effects seem to be significantly transferred from astatine to its neighboring atoms/chemical functions. Apart from the context of chemical reactivity, such transfers are known in the field of NMR (SO-HALA effect).[10–12] For compounds containing one or more heavy atoms, their relativistic behavior can affect the shielding constants of light atoms, particularly regarding the ^{1}H chemical shifts[13,14] and the ^{13}C chemical shifts.[15,16]

In the current work, we aim to investigate the nature of the driving force and the mechanisms supporting the transfer of SOC effects in a molecular environment. For this purpose, we will scrutinize the ability of astatine and of its lighter counterpart, iodine, to form XB interactions with model Lewis bases. In short, XBs are stabilizing interactions that involve a halogen donor, R–X, featuring an electrophilic site associated with the X halogen atom, and a nucleophilic site located on an acceptor, *e.g.*, a Lewis base.[17] The electrophilic region in the outer part of X, referred to as the ''σ-hole'', presents a local deficiency in electron density and can be characterized in terms of the molecular electrostatic potential (V_S).[18] At first, we have chosen R as hydrocarbon chains representative of common motifs found in organic compounds. Then, small dihalogenated inorganic species are studied for probing the influence of the heteroatom electronegativity. As prospect, some original compounds will be finally presented to illustrate extensions of the highlighted phenomena. The Lewis bases used in this work are ammonia, which is recurrently selected as a model partner for theoretical studies on halogen bonding,[19,20] and trimethylamine *N*-oxide, which exhibits a strong XB basicity.[21]

2. Computational methods

In addition to electron correlation effects, relativistic effects have a significant impact on many properties of astatine-containing systems. The SOC can be even stronger for late 6p elements than the scalar-relativistic (sr) effects. The most accurate approach to incorporate relativity would be to perform four-component quantum mechanical calculations based on the exact one-electron relativistic Hamiltonian. Nevertheless, several alternative two-component (2c) approximations have been developed and efficiently used to treat relativistic effects.[22,23] The 2c-relativistic density functional theory (DFT), which was proved to be accurate for studying At-containing systems,[24–27] requires to replace the orbital representation by spinors $\varphi_i(r)$ that are vector functions of two components:

$$\varphi_i(r) = \begin{pmatrix} \varphi_i^{\alpha}(r) \\ \varphi_i^{\beta}(r) \end{pmatrix} = \begin{pmatrix} \sum_{\mu} c_{i\mu}^{\alpha} \chi_{\mu}(r) \\ \sum_{\mu} c_{i\mu}^{\beta} \chi_{\mu}(r) \end{pmatrix} \quad (1)$$

The latter are usually expanded using atom-centered Gaussian basis functions χ_μ, and the expansion coefficients c_i are complex and determined within the variational procedure. The Generalized Kohn–Sham (GKS) method, implemented in the Gaussian 16 program,[28] takes advantages of relativistic pseudo-potentials (PPs) containing scalar and spin-dependent terms. The inclusion of spin-dependent terms into the variational treatment of the one-electron operator ensures that scalar-relativistic and SOC effects are treated on an equal footing. There can be many variations in the form of relativistic PPs. The ones used in this work are expressed as follows:[29]

$$\hat{V}(r) = -\frac{Z_{\text{eff}}}{r} + \sum_{klj} B_{lj}^{k} \exp\left(-\beta_{lj}^{k} r^{2}\right) \hat{P}_{lj} \quad (2)$$

where Z_{eff} is the charge of the inner-core. The sum runs over a Gaussian expansion (index k) of semi-local short-range radial potentials, which are different for different orbital angular-momentum quantum numbers l, and, for a given l, for the two total one-electron angular-momentum quantum numbers $j = l \pm 1/2$. $\hat{P}_{ij}$ is the 2c projector onto the entire space of functions with angular symmetry l, j around the core under study. The parameters B_{lj}^{k} and β_{lj}^{k} are adjusted so that $\hat{V}$ in 2c valence-only atomic calculations reproduces, as closely as possible, a set of relativistic all-electron multiconfiguration Dirac–Hartree–Fock (MCDHF) energies. Note that a transcription of such kind of pseudo-potentials into a spin-averaged part (averaged relativistic potential $\hat{V}_{\text{AREP}}$) and an effective one-electron spin–orbit operator ($\hat{V}_{\text{SO}}$) is easily possible.[30] The omission of $\hat{V}_{\text{SO}}$ in the calculations leads to a scalar-relativistic approach. Hence, SOC effects can readily be quantified *via* the difference between calculations with $\hat{V}_{\text{SO}}$ included in the PPs, and calculations without $\hat{V}_{\text{SO}}$ included in the PPs. To evaluate the SOC effects on studied species, geometry optimizations and frequency calculations have been done at both sr- and 2c-relativistic DFT levels. Vibrational harmonic frequencies were used to establish the nature of the structures (minima *vs.* transition states).

The hybrid B3LYP and meta-hybrid PW6B95 functionals have been selected,[31,32] since they have been recommended in a recent benchmark study focused on At-species,[27] and have been furthermore validated as reliable for investigating compounds stabilized by At-mediated XBs.[9,33–36] The small core pseudo-potentials ECP*n*MDF with n = 60 and 28 were used for the At and I atoms, respectively.[29,37] The explicitly treated electrons were described by a set of triple zeta quality basis sets, abbreviated as TZVPD. We selected the dhf-TZVP-2c basis sets for the At and I atoms,[38] and the def2-TZVP basis sets for the remaining atoms,[39] with diffuse functions being added on all non-H atoms.[40] The energies of the XB complexes were corrected from the basis set superposition error (BSSE) using the counterpoise method,[41] and the corresponding interaction energies were calculated using the super-molecule approach. Note that the results discussed thereafter are mainly from the B3LYP/TZVPD calculations. In order to assess the reliability of previously calculated interaction energies, further *ab initio* calculations were performed on both sr- and 2c-PW6B95/TZVPD geometries. The sr- and 2c-MP2 methods, implemented using the resolution

of the identity technique in the TURBOMOLE program,[42] were used in conjunction with the previously described PPs. We selected a larger set of polarization functions for the basis sets, *i.e.* we used the dhf-TZVPP-2c basis sets for the At and I atoms,[38] and the def2-TZVPP basis sets for the remaining atoms,[39] with diffuse functions being added on all non-H atoms.[40] The semi-core 4s4p4d electrons of I and 5s5p5d electrons of At were kept frozen.

3. Results and discussion

In the coming analysis, two considerations regarding the SOC effects on atomic properties of astatine will be particularly relevant:

(i) a marked decrease (∼8%) of astatine electronegativity χ(At) has been shown when the SOC is taken into account in the quantum mechanical calculations.[27] Note that this weakening is expected to be due to the destabilization by SOC of the valence $6p_{3/2}$ subshell. For instance, both the ionization potential (IP) and the electron affinity (EA) of astatine are decreased by the $6p_{3/2}$ destabilization, and, according to Mulliken's definition of electronegativity (the arithmetic mean of IP and EA), χ(At) must decrease.

(ii) the SOC enhances the propensity of astatine to form charge-shift (CS) bonds.[35,36,43] CS bonds form a class of bonds that emerged recently alongside the two traditional covalent and ionic bond families.[44] CS bonding consists in a large and dynamic fluctuations of the bonding electron-pair, resulting in an important resonance energy between the covalent and ionic structures ($^{-}$A| B^{+} ↔ A–B ↔ $^{+}$A |B^{-}). These features can be characterized through valence bond (VB) and quantum chemical topology (QCT) studies. "Atoms [...] that are prone to CS bonding are compact electronegative and/or lone-pair-rich species, albeit with moderate electronegativity".[45] The atomic propensity for CS bonding was notably traced back to the compactness of valence orbitals.[46] The dominant shrinkage of the $6p_{1/2}$ shell upon inclusion of SOC, ∼0.2 Å with respect to the $6p_z$ orbital,[47] supports the enhanced ability of astatine to form CS bonds.

3.1 Mechanisms for transferring SOC effects

In this section, we have investigated the ability of dihalogenated hydrocarbons At–R–I to form XBs mediated either by the astatine atom (At–XB), or by the iodine one (I–XB). The R group is either a saturated alkyl linear chain or unsaturated alkene or alkyne moieties. Hence, R represents skeletons present in many organic compounds, giving us clues to the mechanisms that can operate in such molecular environments.

Dihalogenated alkanes. A systematic conformational analysis of the dihalogenated methane, ethane, propane and butane monomers leads to one, two, four and twelve energetic minima, respectively. Fig. S1 in the ESI† displays the predicted structures with their respective Boltzmann populations estimated at 25 °C. For the sake of simplicity, we have selected only the two most stable conformers in the case of the butane derivative (h and i in Fig. S1, corresponding to 39.3% of the sample, ESI†). The geometries of XB complexes have then been determined between each conformer of these dihalogenated alkanes and

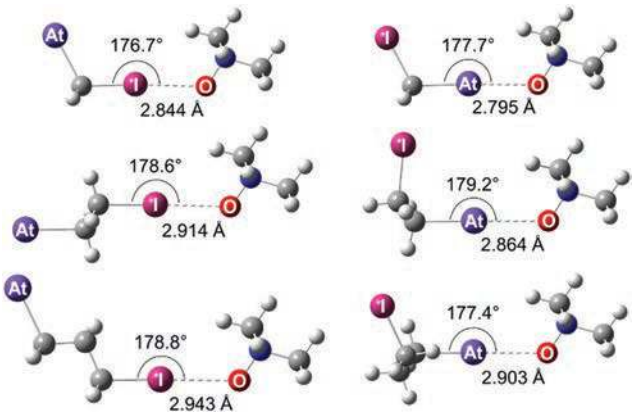

Fig. 1 Calculated structures at the 2c-B3LYP/TZVPD level of theory for the XB complexes formed by some conformers arising from dihalogenated methane (top), ethane (middle) and propane (bottom).

the trimethylamine *N*-oxide (Me_3NO) Lewis base. Some of them are displayed in Fig. 1, illustrating both the possible occurrence of At- and I-mediated interactions, and the conformational flexibility of some XB donors. All studied complexes show interaction distances (d_{int}) between the X = I or At atom and the O atom of the Lewis base, that are shorter than the sum of the van der Waals radii (at least by 15%). Moreover, the angle between the C–X bond and the O atom is always close to 180°, *i.e.* C, X and O are aligned. These features are typical signatures of XB complexes. A Boltzmann population analysis is presented in Table S1 (ESI†), showing for the ethane derivatives that only XB complexes are formed when the At and I atoms are in *anti* position. For the propane and butane derivatives, the studied XB complexes exhibit in contrast well-balanced populations whatever the conformation of the XB donor is.

In Table 1, the interaction energies (ΔE) and distances are evaluated, for a given set of XB complexes, as a weighted average according to the eqn (3) and the Boltzmann populations, p_i, from Table S1 (ESI†).

$$A = \sum_i p_i A_i \qquad (3)$$

For a given R alkyl group, the At–XBs are systematically and significantly stronger than the I–XBs. For example, the interaction energies of the I–XB and the At–XB between At–CH_2–I and Me_3NO are −20.4 and −32.6 kJ mol^{-1}, respectively. This result is in line with the assumption, commonly assumed in the field of halogen bonding, that the propensity of a halogen atom to form XB interactions increases with increasing atom polarizability and decreasing atom electronegativity.[19,49–51] Furthermore, the most electronegative iodine element attracts the electron density toward itself, therefore depopulating astatine and increasing its electrophilicity, *i.e.* enhancing both the astatine σ-hole and its XB-donating ability. The trend on interaction energies is supported by the calculated normalized interaction distances (Table 1). The O···At separation is 21% shorter (r_{XB} = 0.790) than the sum of the van der Waals radii, while the O···I one is 19% shorter (r_{XB} = 0.812), suggesting a stronger interaction between At and O atoms.

Table 1 2c-B3LYP/TZVPD weighted interaction energies and distances, C–X distances and their respective variations upon complexation (X = I, At), for the complexes formed between the dihalogenated alkanes and the trimethylamine *N*-oxide

	ΔE (kJ mol^{-1})	d_{int} (Å)	r_{XB}[a]	d_{C-X} (Å)	Δd_{C-X} (Å)
I–XB	−20.4	2.844	0.812	2.156	0.009
ΔSO[b]	1.8 (8%)	0.020	0.006	0.000	−0.001
At–CH_2–I					
At–XB	−32.6	2.795	0.790	2.316	0.012
ΔSO[b]	−0.7 (−2%)	0.009	0.003	0.043	−0.005
I–XB	−14.6	2.914	0.833	2.223	0.002
ΔSO[b]	1.3 (8%)	0.013	0.004	0.014	−0.004
At–$(CH_2)_2$–I					
At–XB	−26.1	2.850	0.805	2.360	0.012
ΔSO[b]	−1.3 (−5%)	0.001	0.000	0.049	−0.001
I–XB	−13.0	2.962	0.846	2.194	0.005
ΔSO[b]	0.5 (4%)	0.004	0.001	0.005	−0.001
At–$(CH_2)_3$–I					
At–XB	−22.7	2.898	0.819	2.335	0.011
ΔSO[b]	−1.2 (−5%)	−0.001	0.000	0.040	0.000
I–XB	−11.7	2.990	0.854	2.195	0.004
ΔSO[b]	0.2 (2%)	0.002	0.001	0.005	0.000
At–$(CH_2)_4$–I					
At–XB	−20.3	2.927	0.827	2.335	0.008
ΔSO[b]	−1.0 (−5%)	0.000	0.000	0.040	−0.001

[a] Normalized interaction distance $r_{XB} = d_{int}/(r_O + r_X)$; r_O and r_X are the van der Waals radii of the O and X atoms, respectively.[48] A radius of 2.02 Å is assumed for astatine according to sr calculations. [b] The SOC effect (ΔSO) is defined as the difference between the results of 2c and sr calculations.

Upon the R alkyl chain lengthening, we notice a regular weakening of the At–XBs, as well as the I–XBs. The interaction energies in the astatinated complexes change monotonously from −32.6 to −20.3 kJ mol^{-1} with R = CH_2 to $(CH_2)_4$. Indeed, the iodine withdrawing inductive effect (−I) is weakened when R gets longer. The astatine electron density is consequently less depleted, and its XB-donating ability is therefore reduced. The weakening of the I–XBs with the lengthening of the R group is as well significant. ΔE drops from −20.4 to −11.7 kJ mol^{-1} while R = CH_2 to $(CH_2)_4$. The electron donating character of the alkyl groups (+I effect) increases with their lengthening. The enhancement of the +I effect results in more electron density deposit at the iodine atom, and a weakening of its σ-hole. It is worth noting that the R chain lengthening goes along with a systematic decrease of the energy difference between At–XB and I–XB types. The difference ranges from 12.2 to 8.6 kJ mol^{-1} for R = CH_2 to $(CH_2)_4$.

In order to scrutinize the SOC effects, these systems have been as well studied at the scalar relativistic level of theory, the corresponding sr-B3LYP/TZVPD results being gathered in Table S2 in ESI.† In Table 1, the SOC effects (ΔSO) are defined as the difference between 2c-B3LYP/TZVPD and sr-B3LYP/TZVPD results. The At–CH_2–I system exhibits a strong weakening of the I–XB interaction, by 1.8 kJ mol^{-1} (8%), while the effect is opposite and much less important for the At–XB (−0.7 kJ mol^{-1}, *i.e.* a strengthening of 2%). Concluding that the relativistic spin–orbit interaction is much more important on the iodine properties than on those of its heavier analog, astatine, may seem confusing because unexpected (relativistic effects gradually increase with nuclear charge). Actually, the magnitude of the SOC effect on the XB between H–CH_2–I and Me_3NO is only −0.2 kJ mol^{-1}, *i.e.* a weak interaction strengthening of 1% (Table S3 in ESI†). Therefore, it is clear that the resulting SOC effect in At–CH_2–I, which is 10 times more important, can be explained only by the presence of the astatine atom, *i.e.*, the relativistic behavior of astatine's electrons. As previously mentioned, the relativistic spin–orbit interaction significantly decreases the electronegativity of astatine (∼8%).[27] Within the At–CH_2–I species, an electron density redistribution due to SOC occurs from astatine toward the most electronegative iodine atom. This redistribution is evidenced by plotting the difference between electron densities obtained from 2c and sr calculations, as shown in Fig. S2 in ESI.† The charge transfer leads to an electron density increase on iodine, filling in part the density deficiency at the iodine σ-hole. The maximum value of the molecular electrostatic potential, $V_{S,max}$, computed on the extension of the R–X bond, is a descriptor commonly used to quantify the σ-hole strength.[18,19] The $V_{S,max}$ value at the iodine σ-hole decreases by 7% upon SOC (see Fig. S3 in ESI†), leading to a weakening of the I-mediated XB as emphasized above (by 8%). In contrast, the charge transfer due to the SOC reduces the electron density on the astatine atom, which leads to an enhancement of its σ-hole (see Fig. S3, ESI†) and, therefore, to a strengthening of the At-mediated XB (by 2%).

The same behavior is observed for the At–$(CH_2)_2$–I species, *i.e.* the SOC effects do not increase in the sequence X = I to At. However, their magnitudes are close for the two types of XBs; a 8% weakening is found for the I–XB interaction energy and a 5% strengthening for the At–XB. With a further alkyl chain lengthening, we even observe an inversion in the case of At–$(CH_2)_3$–I. The SOC effects are more important on the At–XB (strengthening of 5%) than on the I–XB (weakening of 4%). The −I effect of the iodine atom becoming less pronounced on the astatine atom, we anticipate an attenuation of the electron density migration, induced by SOC, from astatine to iodine. With At–$(CH_2)_4$–I, the SOC effect on the I-mediated XB is indeed markedly reduced. The interaction energy is then affected by only 0.2 kJ mol^{-1} (*i.e.* 2%), which is quite similar to the value obtained for the non-astatinated species, H–$(CH_2)_4$–I (change of −0.1 kJ mol^{-1}, *i.e.* 2%). Therefore, we can conclude that beyond two C–C bonds (R = $(CH_2)_3$), the influence of the spin–orbit interaction induced by astatine's electrons becomes negligible.

Dihalogenated alkenes. After illustrating how, within a molecule, the inductive effects can transfer the consequences of relativistic effects intrinsic to a heavy atom, we can now wonder whether the mesomeric effects can also lead to such a transfer. In the At–R–I series of XB-donors, we have investigated the case where R is a conjugated linear alkene group, starting with vinyl (*Z* and *E*), then the *trans*-buta-1,3-dienyl and finally the *trans*-hexa-1,3,5-trienyl. The characteristics of the XB complexes formed between Me_3NO and At–CH═CH–I do not seem to be so much influenced by the configuration of the XB donor, *i.e. Z* or *E* isomers (see Table S4 in ESI†). The following analysis is therefore focused on the isomers with the two halogens in *anti* position.

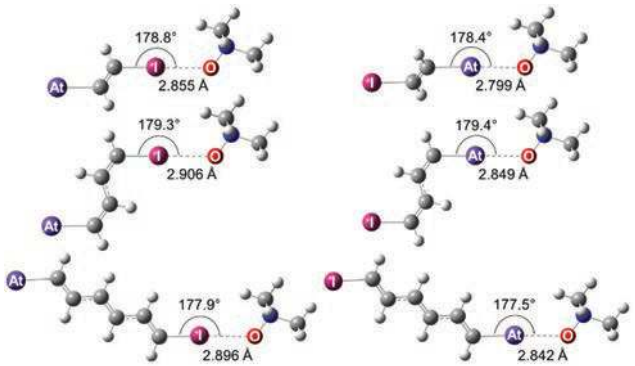

Fig. 2 Calculated structures at the 2c-B3LYP/TZVPD level of theory for the XB complexes formed between At–CH═CH–I, At–(CH═CH)$_2$–I and At–(CH═CH)$_3$–I with the Me$_3$NO Lewis base.

Table 2 2c-B3LYP/TZVPD interaction energies, normalized interaction distances, C–X distances and their respective variations upon complexation (X = I, At), for the complexes formed between dihalogenated alkenes and trimethylamine *N*-oxide

	ΔE (kJ mol^{-1})	r_{XB}[a]	$d_{C\text{–}X}$ (Å)	$\Delta d_{C\text{–}X}$ (Å)
I–XB	−19.7	0.816	2.138	0.012
ΔSO[b]	1.4 (7%)	0.004	0.010	−0.003
At–CH═CH–I				
At–XB	−32.6	0.791	2.280	0.025
ΔSO[b]	−1.3 (−4%)	0.001	0.045	0.001
I–XB	−16.7	0.830	2.117	0.018
ΔSO[b]	0.6 (3%)	0.001	0.005	0.000
At–(CH═CH)$_2$–I				
At–XB	−27.2	0.805	2.261	0.029
ΔSO[b]	−1.1 (−4%)	−0.001	0.039	0.002
I–XB	−17.3	0.828	2.107	0.009
ΔSO[b]	0.2 (1%)	0.001	0.004	0.000
At–(CH═CH)$_3$–I				
At–XB	−27.8	0.803	2.249	0.019
ΔSO[b]	−1.4 (−5%)	−0.001	0.038	0.001

[a] Normalized interaction distance $r_{XB} = d_{int}/(r_O + r_X)$; r_O and r_X are the van der Waals radii of the O and X atoms, respectively.[48] A radius of 2.02 Å is assumed for astatine according to sr calculations. [b] The SOC effect (ΔSO) is defined as the difference between the results of 2c and sr calculations.

The structures of the formed XB complexes are presented in Fig. 2, and their energetics in Table 2. As it can be observed in Fig. 2, all the investigated systems are XB complexes. Indeed, the C, X and O atoms are almost aligned and the interaction distances (d_{int}) are shorter than the sum of the van der Waals radii for X = I or At and the O atom. As for the alkane series, the XBs involving astatine are stronger than the one mediated by iodine. In the case of XB complexes formed by At–CH═CH–I, the interaction energy is, for instance, −19.7 kJ mol^{-1} for the I–XB and −32.6 kJ mol^{-1} for the At–XB. This trend is also supported by the calculated interaction distances. The O···At separation is 21% shorter (r_{XB} = 0.791) than the sum of the van der Waals radii, while the O···I one is 18% shorter (r_{XB} = 0.816).

Considering the influence of SOC, we found a strong weakening of the interaction energy in the I–XB complex formed by At–CH═CH–I, about 7% (1.4 kJ mol^{-1}), while the interaction energy between H$_2$C═CH–I and Me$_3$NO is only modified by 1% (Table S3, ESI†). The enhancement of the SOC effects on the I–XB formed by At–CH═CH–I can only be explained by the presence of astatine. Note that the spin–orbit interaction reinforces the At–XB, but only by 4% (1.3 kJ mol^{-1}). As mentioned previously, because χ(At) significantly decreases with SOC, part of the electron density is redistributed toward the most electronegative atom, iodine. The SOC-induced electronic redistribution is shown in Fig. S2 (ESI†). Consequently, the astatine σ-hole is strengthened while the iodine one is weakened (*cf.* $V_{S,max}$ values in Fig. S3, ESI†). From an energetic point of view, the magnitude of SOC effect on the XBs formed by At–CH═CH–I is similar to those previously discussed for the At–(CH$_2$)$_2$–I system.

In the case of XB complexes formed by At–(CH═CH)$_2$–I, there is again a noticeable effect of SOC on the I–XB interaction strength, which is decreasing by 0.6 kJ mol^{-1} (3%). However, the dominant effect is the At–XB strengthening, by 1.1 kJ mol^{-1} (4%). Note that the consequences of SOC on the I–XB seem here more pronounced than in the case of the XB-donor At–(CH$_2$)$_4$–I (interaction energy affected by 0.2 kJ mol^{-1}). We can consider that, beyond the withdrawal effect (−I) exerted by the iodine atom, the mesomeric effects and particularly the astatine electron-donor ability (+M) could assist the electron redistribution toward the iodine atom, according to Scheme 1, and therefore the transfer of relativistic effects. In contrast, the electron redistribution due to SOC becomes unimportant for the At–(CH═CH)$_3$–I system. In this case, the SOC effects on the I–XB interaction energy is 0.2 kJ mol^{-1} (1%), which is similar to the effect observed with H–(CH═CH)$_3$–I (0.2 kJ mol^{-1}, Table S3, ESI†). Thus, the consequences on iodine of the spin–orbit interaction initiated at the astatine atom, become negligible beyond two conjugated C═C bonds separating the two halogens.

Dihalogenated alkynes. In order to further investigate the assumption on the contribution of mesomeric effects on the electron density redistribution, we also considered At–R–I donors derived from conjugated alkynes. In this series, XB complexes formed between the Me$_3$NO Lewis base and linear dihalogenated alkynes, derived from acetylene, but-1,3-diyne and hexa-1,3,5-triyne, have been studied. The geometrical parameters and energies of these complexes are presented in the Fig. 3 and Table 3, respectively.

Stronger interactions are, again, evidenced when astatine is the halogen atom involved in the XB since the associated ΔE values are more negative (< −50.7 kJ mol^{-1}). Furthermore, the normalized interaction distances, r_{XB}, are systematically shorter for At–XBs (< 0.756). It is also remarkable that both At–XBs and I–XBs strengthen when R gets longer. For instance, the interaction energy of I–XBs monotonously range from −33.4 to −39.2 kJ mol^{-1} when R = C≡C to (C≡C)$_3$. Indeed, the R lengthening increases the number of ethynyl groups that

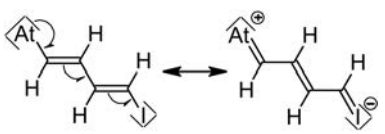

Scheme 1 Mesomeric effects in At–(CH═CH)$_2$–I.

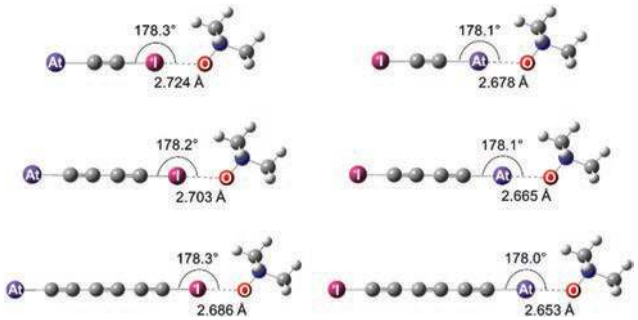

Fig. 3 Calculated structures at the 2c-B3LYP/TZVPD level of theory for the XB complexes formed by At–C≡C–I (top), At–(C≡C)$_2$–I (middle) and At–(C≡C)$_3$–I (bottom) with Me_3NO.

are known as electron-withdrawing groups.[52] As a result, σ(At) and σ(I) become more pronounced. The evolution of the interaction energy goes along with a reduction of the interaction distances, as observed in Fig. 3.

We now focus on SOC effects on the XB interactions, at first in the case of At–C≡C–I as donor. From an energetic point of view, the effects are of similar magnitude for the two types of XB, about 3% (Table 3). This result gives hints to noticeable consequences on iodine resulting from the astatine relativistic behavior. Indeed, the SOC effect is only 1% on the interaction energy between H–C≡C–I and Me_3NO (Table S3, ESI†). This influence through space of relativistic effects, in particular on σ(I) which is strengthened (Fig. S3, ESI†), can be traced back again to the astatine electronegativity decrease due to SOC. However, the transfer appears weakened compared to the case of the alkene counterpart, At–CH=CH–I. The I–XB was then affected by 7% and the At–XB by 4% (Table 2), leading to a differential in favor of iodine of 3% (here for At–C≡C–I, 0%).

Table 3 2c-B3LYP/TZVPD interaction energies, normalized interaction distances, C–X distances and their respective variations upon complexation (X = I, At), for the complexes formed between dihalogenated alkynes and trimethylamine *N*-oxide

	ΔE (kJ mol^{-1})	r_{XB}[a]	$d_{C\text{-}X}$ (Å)	$\Delta d_{C\text{-}X}$ (Å)
I–XB	−33.4	0.778	2.038	0.037
ΔSO[b]	1.1 (3%)	0.002	0.005	−0.001
At–C≡C–I				
At–XB	−50.7	0.756	2.200	0.059
ΔSO[b]	−1.4 (−3%)	0.001	0.049	0.003
I–XB	−36.8	0.772	2.029	0.038
ΔSO[b]	0.4 (1%)	0.001	0.005	0.000
At–(C≡C)$_2$–I				
At–XB	−53.5	0.753	2.192	0.052
ΔSO[b]	−1.7 (−3%)	0.000	0.049	−0.004
I–XB	−39.2	0.767	2.027	0.038
ΔSO[b]	0.3 (1%)	0.000	0.005	−0.285
At–(C≡C)$_3$–I				
At–XB	−55.9	0.750	2.192	0.061
ΔSO[b]	−1.7 (−3%)	0.000	0.050	0.004

[a] Normalized interaction distance $r_{XB} = d_{int}/(r_O + r_X)$; r_O and r_X are the van der Waals radii of the O and X atoms, respectively.[48] A radius of 2.02 Å is assumed for astatine according to sr calculations. [b] The SOC effect (ΔSO) is defined as the difference between the results of 2c and sr calculations.

Regarding the At–(C≡C)$_2$–I and At–(C≡C)$_3$–I species, the I–XBs with Me_3NO are weakened by 1% upon SOC. The magnitude of the SOC effect on the corresponding I–XB with H–(C≡C)$_3$–I is also of 1% (Table S3, ESI†), suggesting that the electron redistribution induced by SOC from astatine to iodine is quenched. Hence, the enhanced π system existing in alkynes does not seem to improve the transfer of SOC effects *via* mesomeric effects, with respect to the previous dihalogenated alkenes.

As an intermediate conclusion, we note that the investigation of the XB-donating ability of some dihalogenated alkanes, alkenes and alkynes shows more pronounced SOC effects on iodine properties than on those of astatine. This finding is at variance with the statement that the relativistic behavior gradually strengthens with the nuclear charge. However, the B3LYP/TZVP results are fully supported by computed interaction energies at the PW6B95/TZVPD and MP2/TZVPPD levels of theory. The latter are presented in Table S5 in ESI† for the XB complexes between At–C_2H_{2n}–I (n = 0, 1, 2) and Me_3NO. The inductive and mesomeric effects were found to help delocalizing the consequences of the spin–orbit interaction initiated by astatine electrons. These mechanisms arise from the decrease of χ(At) with SOC. The connection with electronegativity is further scrutinized in the next section.

3.2 Connection to atomic electronegativities

We have shown that the ability of iodine to form XB interactions can be modulated by relativistic effects originating from a neighboring astatine atom. In this section, we investigate XB interactions between ammonia (NH_3), as Lewis base, and At–AH_n–I (n = 0, 1, 2) species, where atom A is at least divalent and belongs to the second or to the third period of the periodic table of elements, *i.e.* A = Be, B, C, N, O, Mg, Al, Si, P, and S. These elements exhibit either a stronger or a weaker electronegativity than astatine, with a regular evolution within the second and third periods. Hereafter, we will refer to the electronegativity scale recently proposed by Rahm *et al.*,[53] which is consistently based on ground-state energies of valence electrons. Most importantly, this scale takes into account the relativistic spin-dependent effects on the astatine electronegativity. For the elements A = Be, B, Mg, Al and Si, we have χ(A) < χ(At), while for A = C, N, O and S, χ(A) > χ(At). Note that χ(P) ≈ χ(At). Our 2c-B3LYP/TZVPD results show that most of the adducts between ammonia and At–AH_n–I are typical XB complexes. The interaction distances are shorter than the sum of the van der Waals radii of N and X = At or I (see Table S6 in ESI†). Additionally, the A, X, and N atoms are always aligned (Table S6, ESI†). However, for A = Be, Al, and Mg, the interactions appear to be very weak (see Fig. S4 in ESI†) and the associated distances can be up to 18% longer than the sum of the van der Waals radii.

General and expected trends can be identified from the interaction energies calculated at the 2c-B3LYP/TZVPD level of theory (Fig. S4a, ESI†). The At–XB is stronger than the I–XB for a given XB donor, as previously mentioned for dihalogenated hydrocarbons. Furthermore, both the At–XB and the I–XB are strengthened when the electronegativity of the A atom increases.

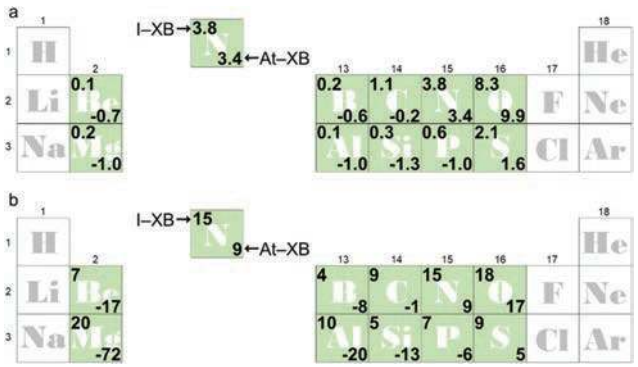

Fig. 4 SOC effects in kJ mol^{-1} (a) and in % (b), on the B3LYP/TZVPD interaction energies calculated for the XB complexes formed between NH_3 and At–AH_n–I species (A = Be, B, C, N, O, Mg, Al, Si, P, S and n = 0, 1, 2).

For instance, considering the second period of the table of elements, the interaction energies of the At–XBs range from −4.9 to −48.8 kJ mol^{-1} when A = Be to O. The more electron-withdrawing ability of the residue bound to the halogen, the larger the halogen σ-hole and the stronger the interaction with Lewis bases.[51,54]

Focusing on the influence of SOC on the computed interaction energies, we notice that the I–XBs are systematically weakened. The results in Fig. 4 show for example that SOC weakens these interactions through the second period by 0.1 to 8.3 kJ mol^{-1} when A = Be to O. As discussed previously, owing to the decrease of χ(At) upon SOC, a part of the electron density attached to astatine is redistributed toward more electronegative atoms or groups. Therefore, the electron density of the AH_n–I moiety is increased and the σ-hole at the iodine extremity is decreased (*cf.* 7% decrease in At–CH_2–I, Fig. S3, ESI†). As an overall trend, we note that the more electronegative the A atom, the more SOC weakens the I–XB interactions. For instance, Fig. 4a shows in the group of chalcogen elements a weakening of the I-mediated XB with ammonia by 2.1 kJ mol^{-1} when A = S, and by 8.3 kJ mol^{-1} when A = O. Indeed, the electron redistribution induced by SOC toward the AH_n–I moiety is enhanced for stronger χ(A). As a result, the electron density in the neighborhood of iodine becomes increasingly important and the σ(I) weaker (compare for instance At–CH_2–I and At–O–I in Fig. S2, ESI†).

Regarding the role of SOC on At–XBs, we notice a strengthening of the interaction when χ(A) is lower or close to χ(At). For example, the SOC enhances the interaction on average by 1.1 kJ mol^{-1} through the third period from A = Mg to P (Fig. 4a). As stated earlier, the SOC induces a migration of the electron density toward the AH_n–I moiety, reducing the electron density attached to astatine. Consequently, the astatine σ-hole is strengthened (*i.e.* its propensity to form XB interaction). When A is more electronegative than astatine, χ(A) > χ(At), it may seem surprising to find that the SOC generally weakens the At–XBs: the interaction energies is reduced by 1.6, 3.4, and 9.9 kJ mol^{-1} for A = S, N and O (Fig. 4a), respectively. This behavior cannot be explained by the mechanisms of electron density redistribution due to astatine electronegativity decrease under SOC influence. However, astatine is known to be subject to CS bonding and this ability is affected by the SOC.[43,55] We have shown in previous studies that CS mechanism weakens the XB-donating ability of astatine,[35,36] notably due to the decrease of the local electrophilicity at its σ-hole. Furthermore, according to the established trends on CS bonding,[44,45] the CS character of the A–At bond raises when atom A becomes more electronegative and/or lone-pair rich. A significant contribution of CS bonding is therefore expected for the A–At bonds when χ(A) > χ(At), and this contribution is enhanced by SOC, which further weakens the astatine propensity to form XB (for example, the most positive electrophilicity value, $\omega^{+}_{s,max}$, at σ(At) in At–S–I species is reduced by 30% upon SOC, see Fig. S5 in ESI†).

The most important point is that, for a given At–AH_n–I species and when χ(A) ≥ χ(At), the influence of the spin–orbit interaction on the I–XB is stronger than that on the At–XB. The evolution of SOC effects on the interaction energies, as a function of the electronegativity of atom A, is depicted in Fig. S6 in ESI.† The magnitude of the effects on the I–XB can be larger in relative value (Fig. 4b, A = P, S, C, N and O) and even in absolute value (Fig. 4a, A = S, C and N). These findings again testify to a significant transfer through space of the consequences of the astatine's relativistic behavior. This transfer arises necessarily from a redistribution upon SOC of some of the astatine electron density toward iodine. The preceding discussion tells us that this mechanism is amplified with the A electronegativity increase, which therefore intensifies the weakening with SOC of the XB-donating ability of iodine. One would also expect that amplifying the electronic redistribution would intensify the strengthening with SOC of the XB-donating ability of astatine. How can the magnitude of SOC effects be less on astatine? It supposedly requires a second mechanism that opposes the strengthening of the XB-donating ability of astatine. This is achieved by the CS character increase of the A–At bond, accompanying the A electronegativity increase. Indeed, the CS bonding mechanism restrains astatine to form XB interactions and notably prevails when χ(A) > χ(At) (SOC essentially weakens the At–XBs in this case). Consequently, the SOC effects on the At–XBs are smaller when χ(A) ≥ χ(At), with respect to those on the XBs mediated by iodine. Note that the trends disclosed from the results of B3LYP/TVZP calculations are well corroborated by further PW6B95/TZVPD and MP2/TZVPPD calculations. Table S7 in ESI† notably presents some interactions energies computed for XB complexes formed by ammonia with the At–AH_n–I species (A = B, C, N and O).

3.3 Prospects

In this section, we wish to illustrate by combinations of the mechanisms described previously, how chemists could control the transfer of relativistic effects. Significant enhancements can be achieved by introducing usual chemical functions, in particular for the above compounds. From the At–CH_2–I model, one can combine conjugation and electron-withdrawing effect by introducing a carbonyl group. Indeed, the At–C(═O)–I species is planar and the SOC-induced electronic redistribution can takes advantage of −M effects. The characteristics of the formed XB complexes with NH_3 are presented in Table 4. First, the XB interactions are stronger

Table 4 2c-B3LYP/TZVPD interaction energies and distances upon complexation (X = I, At), for the complexes formed by the NH_3 Lewis base with the At–C(=O)–I, At–SO–I and At–S(=O)$_2$–I species

	ΔE (kJ mol^{-1})	d_{int} (Å)	r_{XB}[a]
I–XB	−14.2	3.030	0.866
ΔSO[b]	3.4 (19%)	0.052	0.015
At–C(=O)–I			
At–XB	−26.0	2.943	0.831
ΔSO[b]	0.0 (0%)	0.025	0.007
I–XB	−25.8	2.812	0.803
ΔSO[b]	7.2 (22%)	0.074	0.021
At–S(=O)$_2$–I			
At–XB	−42.1	2.784	0.786
ΔSO[b]	3.8 (8%)	0.066	0.019

[a] Normalized interaction distance $r_{XB} = d_{int}/(r_N + r_X)$; r_N and r_X are the van der Waals radii of the N and X atoms, respectively.[48] A radius of 2.02 Å is assumed for astatine according to sr calculations. [b] The SOC effect (ΔSO) is defined as the difference between the results of 2c and sr calculations.

than with At–CH_2–I as XB donor (more negative ΔE values and shorter d_{int} distances). While the energy of the At–XB is unchanged by SOC, the I–XB is weakened by 3.4 kJ mol^{-1} (19%). Hence, the influence of SOC on the I–XB strength is at least twice as large as in the case of the analogous interaction formed by At–CH_2–I (*cf.* Fig. 4, ΔSO = 1.1 kJ mol^{-1}, *i.e.*, 8%). Here, the substitution by a simple carbonyl group greatly facilitates the delocalization of the consequences of the spin–orbit interaction initiated by astatine's electrons.

Note that rather than carbon, we can think of a heteroatom double-bonded to an oxygen atom for modulating the difference in electronegativity with astatine. The sulfonyl functional group S(=O)$_2$ is found primarily in sulfones, which constitute an important class of organic compounds, and also in many important drugs belonging to the sulfonamide class. Table 4 gathers the results obtained for the XB complexes between NH_3 and At–S(=O)$_2$–I. The inclusion of SOC in calculations weakens the At–XB by 3.8 kJ mol^{-1} (8%), but the I–XB is the most weakened one. Its interaction energy changes by 7.2 kJ mol^{-1} (22%). Hence, a much bigger effect is obtained compared to the I–XB formed by At–C(=O)–I, and also to that formed by At–S–I (*cf.* Fig. 4, ΔSO = 2.1 kJ mol^{-1}, *i.e.*, 9%). The substituted sulfur atom significantly promotes the transfer of the relativistic effects on iodine properties.

Another option for acting on the delocalization of relativistic effects is to consider the possible presence of several heavy elements such as astatine. Additive and synergetic effects can be expected. This possibility was evaluated by considering the formation of XB complexes between the Me_3NO Lewis base and perhalogeno-cumulene derivatives, which possibly allows comparisons with the dihalogenated hydrocarbons studied previously. Cumulenes are hydrocarbons with cumulative and consecutive double bonds, which prevents any resonance (the consecutive π bonds are perpendicular to each other). Their distinctive electronic structure makes them appealing for molecular nanotechnology, notably as molecular wires.[56] Fig. 5a displays the structures of XB complexes obtained with a hexapentaene derivative. In the XB donor, the two astatine atoms are equivalent and the At-mediated XB, of 46.9 kJ mol^{-1}, is almost unaffected when the calculations take into account the spin–orbit interaction. Indeed, the interaction energy is only modified by 0.4 kJ mol^{-1} (1%). The two iodine atoms are also equivalent in the XB donor but, in contrast, the SOC effect on the I–XB is about four times bigger. The interaction energy changes by 1.5 kJ mol^{-1} (4%), and finally settles at −33.3 kJ mol^{-1}. The transfer of the relativistic effects is obvious despite the absence of resonance in this planar XB-donor, and even though the astatine and iodine atoms are spaced five carbon–carbon bonds apart. This is much longer than the limits previously established in the case of dihalogenated hydrocarbons (*e.g.* two C–C bonds for alkanes, and two conjugated C=C bonds for alkenes). Hence, heavy elements can demonstrate within a compound a synergetic behavior that significantly supports the transfer of relativistic effects towards a distant chemical function.

So far, we have evaluated the influence of astatine on I-mediated XBs where both the iodine and astatine atoms belong to the XB-donor species. Still considering the influence of astatine on I–XBs, one can wonder its impact on XB-acceptor chemical functions. Very recently, Joy *et al.* have studied some I-mediated interactions involving XB acceptors belonging to the family of propellanes.[57] Propellanes are cyclic hydrocarbons that possess a variety of interesting structural and electronic features, notably an inverted tetrahedral arrangement of their bridgehead carbon atoms. The nature of the central bond between the bridgehead atoms in [1.1.1]propellane is particularly debated, the latter falling in the class of CS bonds according to VB and QCT studies by Shaik and co-workers.[44] The bridgehead carbons are powerful nucleophilic sites,[57] as well as "very-light" atoms *vs.* astatine. We intend to compare XBs formed by diiodine (I_2) with [1.1.1]-propellane and perastato-[1.1.1]propellane. Fig. 5b and c displays the structures of the XB complexes. Diiodine is bound to the perastato-[1.1.1]propellane by 7.6 kJ mol^{-1}, and this binding mainly results from the spin–orbit interaction. Indeed, the SOC contributes by 5.0 kJ mol^{-1} to the interaction energy. However, this significant strengthening of the I–XB is disconnected from

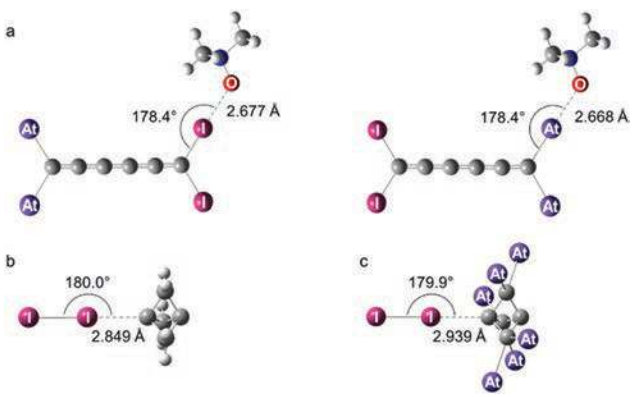

Fig. 5 Calculated structures at the 2c-B3LYP/TZVPD level of theory for the XB complexes between (a) 1,1-diastato-6,6-diiodohexapentaene and trimethylamine *N*-oxide, (b) diiodide and [1.1.1]propellane, and, (c) diiodide and perastato-[1.1.1]propellane.

the relativistic character of iodine. The SOC effect on the XB interaction between I_2 and unsubstituted [1.1.1]propellane is actually smaller by one order of magnitude (0.6 kJ mol^{-1}), and weakens the interaction energy to 18.7 kJ mol^{-1}. Hence, the strong strengthening, with SOC, of the I–XB between diiodine and perastato-[1.1.1]propellane arises only from the astatine atoms, while they are not bonded to the interacting atoms. The XB basicity of the bridgehead carbons in perastato-[1.1.1]-propellane is emphasized by the relativistic behavior of the many astatines. This latest study confirms that, within a compound, the chemical properties of light elements, such as carbon, can be more affected by relativistic effects than those of the heavy elements, such as iodine and astatine, which are the source of these effects.

4. Conclusions

Relativistic effects are defined as the differences between results of physical models that consider and that do not consider relativity. In this computational investigation, we focused on the influence of the spin–orbit coupling on halogen-bond interactions involving compounds bearing iodine and astatine atoms. In several cases, the halogen bonds mediated by astatine were found less affected than their counterparts mediated by iodine. This finding appears confusing at first because relativistic effects are expected to be increasingly important with the atomic nuclear charge, and iodine ($Z = 53$) is a lighter analog of astatine ($Z = 85$). This behavior is explained by a transfer toward iodine of the consequences of the relativistic spin–orbit interaction initiated by astatine electrons. The underlying mechanisms that support this through-space transfer have been identified:

(i) an increased difference of electronegativity, when relativity is active, allowing a redistribution of part of astatine electron density to iodine

(ii) the inductive effects (−I) of the chemical backbone, which can help to propagate between astatine and iodine the electronic redistribution up to two C–C bonds

(iii) electron-withdrawing mesomeric effects (−M), which can add to (or quench) the above mechanisms

Because features (ii) and (iii) are rather common in chemical compounds, the transfer of relativistic effects from a heavy atom to a distant light atom/chemical function is a reality. Although currently not sought after, delocalized relativistic effects were at least evidenced for astatine monoiodide (AtI),[9] which is currently the reference donor for the experimental basicity scale of At-mediated halogen bonds.[33,34] The effects can be significant; we have found the halogen-bond basicity of a carbon atom to be here more than doubled. Beyond the prospect of using chemical substitutions to modulate the transfer of relativistic effects, it seems important to us notifying that the transfer can be of importance for elements other than astatine. Indeed, the crucial factor is the change of atomic electronegativity, which mainly results from the split of the high-lying valence shell due to the spin–orbit interaction. For neighboring elements bismuth and polonium, the energy split between $6p_{1/2}$ and $6p_{3/2}$ subshells is also important, making them possible ''donors'' of relativistic effects. The same should hold for recently synthesized late-7p elements, *e.g.*, moscovium, livermorium and tennessine.

Conflicts of interest

There are no conflicts to declare.

Acknowledgements

This work has been in part supported by grants from the French National Agency for Research called ''Investissements d'Avenir'', Equipex Arronax-Plus (ANR-11-EQPX-0004), Labex IRON (ANR-11-LABX-18-01) and ISITE NExT (ANR-16-IDEX-0007). It was carried out using HPC resources from CCIPL (''Centre de Calcul Intensif des Pays de la Loire'').

Notes and references

1 G. N. Lewis, The Atom And The Molecule, *J. Am. Chem. Soc.*, 1916, **38**, 762–785.
2 P. A. M. Dirac, Quantum mechanics of many-electron systems, *Proc. R. Soc. A*, 1929, **123**, 714–733.
3 W. Kutzelnigg, Perspective on ''Quantum mechanics of many-electron systems, *Theor. Chem. Acc.*, 2000, **103**, 182–186.
4 S. J. Rose, I. P. Grant and N. C. Pyper, The direct and indirect effects in the relativistic modification of atomic valence orbitals, *J. Phys. B*, 1978, **11**, 1171–1176.
5 W. H. E. Schwarz, E. M. van Wezenbeek, E. J. Baerends and J. G. Snijders, The origin of relativistic effects of atomic orbitals, *J. Phys. B: At., Mol. Opt. Phys.*, 1989, **22**, 1515–1529.
6 E. J. Baerends, W. H. E. Schwarz, P. Schwerdtfeger and J. G. Snijders, Relativistic atomic orbital contractions and expansions: magnitudes and explanations, *J. Phys. B: At., Mol. Opt. Phys.*, 1990, **23**, 3225–3240.
7 K. G. Dyall and K. Faegri, Jr, *Introduction to Relativistic Quantum Chemistry*, Oxford University Press, Oxford, New York, 2007.
8 *Relativistic Methods for Chemists*, ed. M. Barysz and Y. Ishikawa, Springer, Netherlands, 2010.
9 N. Galland, G. Montavon, J.-Y. Le Questel and J. Graton, Quantum calculations of At-mediated halogen bonds: on the influence of relativistic effects, *New J. Chem.*, 2018, **42**, 10510–10517.
10 Y. Nomura, Y. Takeuchi and N. Nakagawa, Substituent effects in aromatic proton NMR spectra. III substituent effects caused by halogens, *Tetrahedron Lett.*, 1969, **10**, 639–642.
11 P. Pyykkö, A. Görling and N. Rösch, A transparent interpretation of the relativistic contribution to the N.M.R. 'heavy atom chemical shift, *Mol. Phys.*, 1987, **61**, 195–205.
12 M. Kaupp, O. L. Malkina, V. G. Malkin and P. Pyykkö, How do spin–orbit-induced heavy-atom effects on NMR chemical shifts function? Validation of a simple analogy to spin–spin

coupling by density functional theory (DFT) calculations on some iodo compounds, *Chem. – Eur. J.*, 1998, **4**, 118–126.
13 L. Visscher, T. Enevoldsen, T. Saue, H. J. A. Jensen and J. Oddershede, Full four-component relativistic calculations of NMR shielding and indirect spin–spin coupling tensors in hydrogen halides, *J. Comput. Chem.*, 1999, 1262–1273.
14 J. Autschbach and S. Zheng, in *Annual Reports on NMR Spectroscopy*, ed. G. A. Webb, Academic Press, 2009, vol. 67, pp. 1–95.
15 S. K. Wolff, T. Ziegler, E. van Lenthe and E. J. Baerends, Density functional calculations of nuclear magnetic shieldings using the zeroth-order regular approximation (ZORA) for relativistic effects: ZORA nuclear magnetic resonance, *J. Chem. Phys.*, 1999, **110**, 7689–7698.
16 Y. Y. Rusakov, I. L. Rusakova and L. B. Krivdin, On the HALA effect in the NMR carbon shielding constants of the compounds containing heavy p-elements, *Int. J. Quantum Chem.*, 2016, **116**, 1404–1412.
17 G. R. Desiraju, P. S. Ho, L. Kloo, A. C. Legon, R. Marquardt, P. Metrangolo, P. Politzer, G. Resnati and K. Rissanen, Definition of the halogen bond (IUPAC Recommendations 2013), *Pure Appl. Chem.*, 2013, **85**, 1711–1713.
18 T. Clark, M. Hennemann, J. S. Murray and P. Politzer, Halogen bonding: the σ-hole, *J. Mol. Model.*, 2007, **13**, 291–296.
19 M. H. Kolář and P. Hobza, Computer Modeling of Halogen Bonds and Other σ-Hole Interactions, *Chem. Rev.*, 2016, **116**, 5155–5187.
20 G. Hoffmann, V. Tognetti and L. Joubert, Electrophilicity Indices and Halogen Bonds: Some New Alternatives to the Molecular Electrostatic Potential, *J. Phys. Chem. A*, 2020, **124**, 2090–2101.
21 C. Laurence, J. Graton, M. Berthelot and M. J. El, Ghomari, The Diiodine Basicity Scale: Toward a General Halogen-Bond Basicity Scale, *Chem. – Eur. J.*, 2011, **17**, 10431–10444.
22 T. Saue, Relativistic Hamiltonians for Chemistry: A Primer, *ChemPhysChem*, 2011, **12**, 3077–3094.
23 J. Autschbach, Perspective: Relativistic effects, *J. Chem. Phys.*, 2012, **136**, 150902.
24 A. V. Mitin and C. van Wüllen, Two-component relativistic density-functional calculations of the dimers of the halogens from bromine through element 117 using effective core potential and all-electron methods, *J. Chem. Phys.*, 2006, **124**, 064305.
25 J. Champion, M. Seydou, A. Sabatié-Gogova, E. Renault, G. Montavon and N. Galland, Assessment of an effective quasirelativistic methodology designed to study astatine chemistry in aqueous solution, *Phys. Chem. Chem. Phys.*, 2011, **13**, 14984–14992.
26 D.-D. Yang and F. Wang, Structures and stabilities of group 17 fluorides EF3 (E = I, At, and element 117) with spin–orbit coupling, *Phys. Chem. Chem. Phys.*, 2012, **14**, 15816–15825.
27 D.-C. Sergentu, G. David, G. Montavon, R. Maurice and N. Galland, Scrutinizing ''Invisible'' astatine: a challenge for modern density functionals, *J. Comput. Chem.*, 2016, **37**, 1345–1354.
28 M. J. Frisch, G. W. Trucks, H. B. Schlegel, G. E. Scuseria, M. A. Robb, J. R. Cheeseman, G. Scalmani, V. Barone, G. A. Petersson, H. Nakatsuji, X. Li, M. Caricato, A. V. Marenich, J. Bloino, B. G. Janesko, R. Gomperts, B. Mennucci, H. P. Hratchian, J. V. Ortiz, A. F. Izmaylov, J. L. Sonnenberg, D. Williams-Young, F. Ding, F. Lipparini, F. Egidi, J. Goings, B. Peng, A. Petrone, T. Henderson, D. Ranasinghe, V. G. Zakrzewski, J. Gao, N. Rega, G. Zheng, W. Liang, M. Hada, M. Ehara, K. Toyota, R. Fukuda, J. Hasegawa, M. Ishida, T. Nakajima, Y. Honda, O. Kitao, H. Nakai, T. Vreven, K. Throssell, J. A. Montgomery Jr., J. E. Peralta, F. Ogliaro, M. J. Bearpark, J. J. Heyd, E. N. Brothers, K. N. Kudin, V. N. Staroverov, T. A. Keith, R. Kobayashi, J. Normand, K. Raghavachari, A. P. Rendell, J. C. Burant, S. S. Iyengar, J. Tomasi, M. Cossi, J. M. Millam, M. Klene, C. Adamo, R. Cammi, J. W. Ochterski, R. L. Martin, K. Morokuma, O. Farkas, J. B. Foresman and D. J. Fox, *Gaussian 16 Rev*. A.03, Wallingford, CT, 2016.
29 K. A. Peterson, D. Figgen, E. Goll, H. Stoll and M. Dolg, Systematically convergent basis sets with relativistic pseudopotentials. II. Small-core pseudopotentials and correlation consistent basis sets for the post-d group 16-18 elements, *J. Chem. Phys.*, 2003, **119**, 11113–11123.
30 M. Dolg and X. Cao, Relativistic Pseudopotentials: Their Development and Scope of Applications, *Chem. Rev.*, 2012, **112**, 403–480.
31 P. J. Stephens, F. J. Devlin, C. F. Chabalowski and M. J. Frisch, Ab Initio Calculation of Vibrational Absorption and Circular Dichroism Spectra Using Density Functional Force Fields, *J. Phys. Chem.*, 1994, **98**, 11623–11627.
32 Y. Zhao and D. G. Truhlar, Design of Density Functionals That Are Broadly Accurate for Thermochemistry, Thermochemical Kinetics, and Nonbonded Interactions, *J. Phys. Chem. A*, 2005, **109**, 5656–5667.
33 L. Liu, N. Guo, J. Champion, J. Graton, G. Montavon, N. Galland and R. Maurice, Towards a Stronger Halogen Bond Involving Astatine: Unexpected Adduct with Bu3PO Stabilized by Hydrogen Bonding, *Chem. – Eur. J.*, 2020, **26**, 3713–3717.
34 N. Guo, R. Maurice, D. Teze, J. Graton, J. Champion, G. Montavon and N. Galland, Experimental and computational evidence of halogen bonds involving astatine, *Nat. Chem.*, 2018, **10**, 428–434.
35 J. Graton, S. Rahali, J.-Y. L. Questel, G. Montavon, J. Pilmé and N. Galland, Spin–orbit coupling as a probe to decipher halogen bonding, *Phys. Chem. Chem. Phys.*, 2018, **20**, 29616–29624.
36 S. Sarr, J. Graton, G. Montavon, J. Pilmé and N. Galland, On the Interplay between Charge-Shift Bonding and Halogen Bonding, *ChemPhysChem*, 2020, **21**, 240–250.
37 K. A. Peterson, B. C. Shepler, D. Figgen and H. Stoll, On the Spectroscopic and Thermochemical Properties of ClO, BrO, IO, and Their Anions, *J. Phys. Chem. A*, 2006, **110**, 13877–13883.
38 F. Weigend and A. Baldes, Segmented contracted basis sets for one- and two-component Dirac–Fock effective core potentials, *J. Chem. Phys.*, 2010, **133**, 174102.

39 F. Weigend and R. Ahlrichs, Balanced basis sets of split valence, triple zeta valence and quadruple zeta valence quality for H to Rn: Design and assessment of accuracy, *Phys. Chem. Chem. Phys.*, 2005, **7**, 3297–3305.

40 D. Rappoport and F. Furche, Property-optimized Gaussian basis sets for molecular response calculations, *J. Chem. Phys.*, 2010, **133**, 134105.

41 S. F. Boys and F. Bernardi, The calculation of small molecular interactions by the differences of separate total energies. Some procedures with reduced errors, *Mol. Phys.*, 1970, **19**, 553–566.

42 TURBOMOLE, a development of University of Karlsruhe and Forschungszentrum Karlsruhe GmbH, 1989–2007, TURBOMOLE GmbH, since 2007, available from http://www.turbomole.com, 2014.

43 J. Pilmé, E. Renault, F. Bassal, M. Amaouch, G. Montavon and N. Galland, QTAIM Analysis in the Context of Quasirelativistic Quantum Calculations, *J. Chem. Theory Comput.*, 2014, **10**, 4830–4841.

44 S. Shaik, D. Danovich, W. Wu and P. C. Hiberty, Charge-shift bonding and its manifestations in chemistry, *Nat. Chem.*, 2009, **1**, 443–449.

45 S. Shaik, D. Danovich, B. Silvi, D. L. Lauvergnat and P. C. Hiberty, Charge-Shift Bonding – A Class of Electron-Pair Bonds That Emerges from Valence Bond Theory and Is Supported by the Electron Localization Function Approach, *Chem. – Eur. J.*, 2005, **11**, 6358–6371.

46 S. Shaik, P. Maitre, G. Sini and P. C. Hiberty, The charge-shift bonding concept. Electron-pair bonds with very large ionic-covalent resonance energies, *J. Am. Chem. Soc.*, 1992, **114**, 7861–7866.

47 F. Réal, A. Severo Pereira Gomes, Y. O. Guerrero Martínez, T. Ayed, N. Galland, M. Masella and V. Vallet, Structural, dynamical, and transport properties of the hydrated halides: How do At^- bulk properties compare with those of the other halides, from F^- to I^-?, *J. Chem. Phys.*, 2016, **144**, 124513.

48 M. Mantina, A. C. Chamberlin, R. Valero, C. J. Cramer and D. G. Truhlar, Consistent van der Waals Radii for the Whole Main Group, *J. Phys. Chem. A*, 2009, **113**, 5806–5812.

49 P. Politzer, P. Lane, M. C. Concha, Y. Ma and J. S. Murray, An overview of halogen bonding, *J. Mol. Model.*, 2007, **13**, 305–311.

50 L. P. Wolters, P. Schyman, M. J. Pavan, W. L. Jorgensen, F. M. Bickelhaupt and S. Kozuch, The many faces of halogen bonding: a review of theoretical models and methods, *Wiley Interdiscip. Rev.: Comput. Mol. Sci.*, 2014, **4**, 523–540.

51 G. Cavallo, P. Metrangolo, R. Milani, T. Pilati, A. Priimagi, G. Resnati and G. Terraneo, The Halogen Bond, *Chem. Rev.*, 2016, **116**, 2478–2601.

52 P. B. D. De La Mare and R. Bolton, *Electrophilic Additions to Unsaturated Systems*, Elsevier Science, Amsterdam, Netherlands, 2nd edn, 2013.

53 M. Rahm, T. Zeng and R. Hoffmann, Electronegativity Seen as the Ground-State Average Valence Electron Binding Energy, *J. Am. Chem. Soc.*, 2019, **141**, 342–351.

54 P. Politzer, J. S. Murray and T. Clark, Halogen bonding: an electrostatically-driven highly directional noncovalent interaction, *Phys. Chem. Chem. Phys.*, 2010, **12**, 7748–7757.

55 C. G. Pech, P. A. B. Haase, D.-C. Sergentu, A. Borschevsky, J. Pilmé, N. Galland and R. Maurice, Quantum chemical topology at the spin–orbit configuration interaction level: Application to astatine compounds, *J. Comput. Chem.*, 2020, **41**, 2055–2065.

56 J. A. Januszewski and R. R. Tykwinski, Synthesis and properties of long[*n*]cumulenes ($n \geq 5$), *Chem. Soc. Rev.*, 2014, **43**, 3184–3203.

57 J. Joy, E. Akhil and E. D. Jemmis, Halogen bond shortens and strengthens the bridge bond of [1.1.1]propellane and the open form of [2.2.2]propellane, *Phys. Chem. Chem. Phys.*, 2018, **20**, 25792–25798.